NANO LETTERS

pubs.acs.org/NanoLett Letter

Xylem-Inspired Polyimide/MXene Aerogels with Radial Lamellar Architectures for Highly Sensitive Strain Detection and Efficient Solar Steam Generation

Lei Pu, Haojie Ma, Jiancheng Dong, Chao Zhang, Feili Lai, Guanjie He, Piming Ma, Weifu Dong, Yunpeng Huang,* and Tianxi Liu*

Cite This: *Nano Lett.* 2022, 22, 4560−4568 Read Online

ACCESS | Metrics & More | Article Recommendations | Supporting Information

ABSTRACT: Polyimide aerogels with mechanical robustness, great compressibility, excellent antifatigue properties, and intriguing functionality have captured enormous attention in diverse applications. Here, enlightened by the xylem parenchyma of dicotyledonous stems, a radially architectured polyimide/MXene composite aerogel (RPIMX) with reversible compressibility is developed by combining the interfacial enhancing strategy and radial ice-templating method. The strong interaction between MXene flakes and polymer can glue the MXene to form continuous lamellae, the ice crystals grow preferentially along the radial temperature gradient can effectively constrain the lamellae to create a biomimetic radial lamellar architecture. As a result, the nature-inspired RPIMX composite aerogel with centrosymmetric lamellar structure and oriented channels manifests excellent mechanical strength, electrical conductivity, and water transporting capability along the longitudinal direction, endowing itself with intriguing applications for accurate human motion monitoring and efficient photothermal evaporation. These exciting properties make the biomimetic RPIMX aerogels promising candidates for flexible piezoresistive sensors and photothermal evaporators.

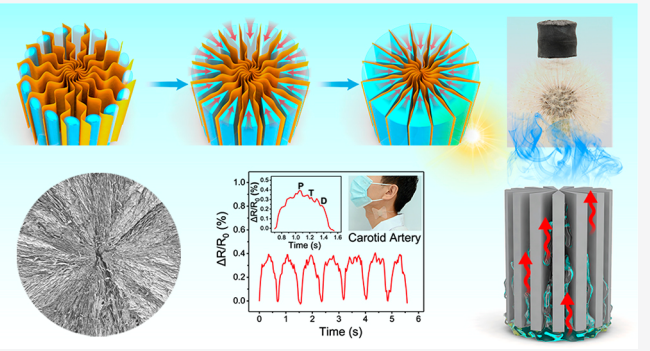

KEYWORDS: *bioinspired, polyimide, MXene, piezoresistive sensor, photothermal evaporation*

Pressure sensors that can convert received forces into electrical signals are widely used in autonomous vehicles, industrial manufacturing automation, artificial intelligence, and healthcare monitoring devices.[1−4] According to different working mechanisms, pressure sensors are mainly divided into piezoresistive, piezoelectric, and capacitive-type.[5,6] Piezoresistive sensors based on the linear change between force-deformation-resistance have been extensively studied and widely used because of their low cost, great operation stability, and high linear response capability.[7−9] Conventional piezoresistive sensors are mostly constructed by metal or inorganic semiconductor materials, which have serious concerns of portability, flexibility, and wearability.[10,11] Therefore, flexible sensors involving flexible conducting materials have received extensive attention in the fields of electronic skin and robots due to their good flexibility, wearability, and real-time monitoring ability.[12] Conductive polymer composites with good compressibility are ideal candidates for flexible piezoresistive sensors,[13−16] which are usually constructed by direct deposition of conductive materials on insulating matrixes via impregnation and sputtering methods.[17] For example, Guo et al.[18] assembled carbon nanotubes (CNTs) on thermoplastic polyurethane (TPU) fibers by ultrasonic-assisted impregnation, obtaining a highly conductive and stretchable yarn with excellent piezoresistive sensing performance. Liu et al.[19] reported a microcracked piezoresistive material with high elasticity and a wide strain range, which was fabricated by sputtering gold nanoparticles on a PU sponge. However, the above sensory materials severely suffered from poor stability due to the cracking and detachment of conductive materials.[20]

Compressive macroscopic foams or aerogels integrating the conductive components with the polymeric matrix are proved to be preferable candidates for flexible piezoresistive sensors. For example, Shen et al.[21] constructed a CNT/epoxy/TPU porous foam with a herringbone structure through a directional freezing method, which showed a good differentiation capability toward different compression strain amplitude. It is well-known that the 3D structures of aerogels are crucial for

Received: April 12, 2022
Revised: May 16, 2022
Published: May 18, 2022

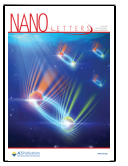

https://doi.org/10.1021/acs.nanolett.2c01486
Nano Lett. 2022, 22, 4560−4568

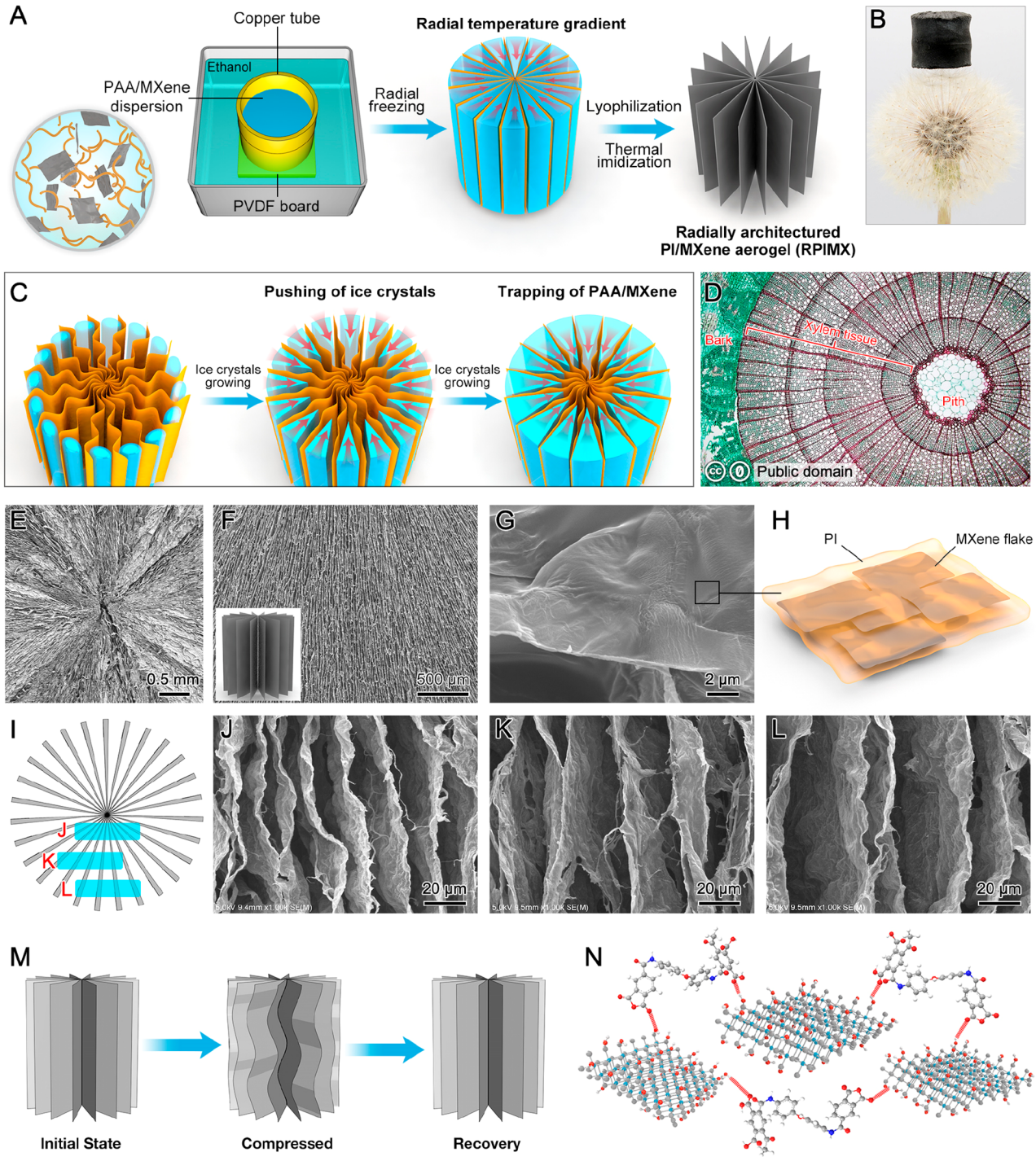

Figure 1. (A) Fabrication process of the radially architectured RPIMX composite aerogels. (B) The lightweight demonstration of the composite aerogel (it can stand steadily on a dandelion). (C) Illustration showing the formation of radiating structures using radial ice-templating strategy. (D) An optical microscope image showing the purple stained xylem tissue of *Liriodendron* stem (Berkshire Community College Bioscience Image Library, licensed under a Public Domain license, https://creativecommons.org/publicdomain/zero/1.0/). (E,F) SEM images showing the transverse section and outer surface morphology of RPIMX composite aerogel. (G,H) SEM image and schematic diagram of single PI/MXene composite lamella. (I–L) Illustration and SEM images showing the decreased width (λ) of the interlayer channels in three regions. (M) Schematic illustration showing the compressing/releasing process of RPIMX composite aerogel. (N) Schematic description of the interfacial interaction between PAA and MXene flakes.

their overall performance, hence, tremendous research works have been devoted to the rational design of various microstructures.[22] Among, aerogels with aligned porous structures are reported to possess superior mechanical properties and electrical conductivity than aerogels with random porosity.[23,24] Sui et al.[25] developed a CNF/SA composite aerogel with aligned 3D porous structure through freeze-drying and Ca^{2+} cross-linking, resulted aligned porous skeletal structure enabled the CNF/SA aerogel with excellent underwater structural stability. In addition, Ruoff et al.[26] used a

https://doi.org/10.1021/acs.nanolett.2c01486
Nano Lett. 2022, 22, 4560−4568

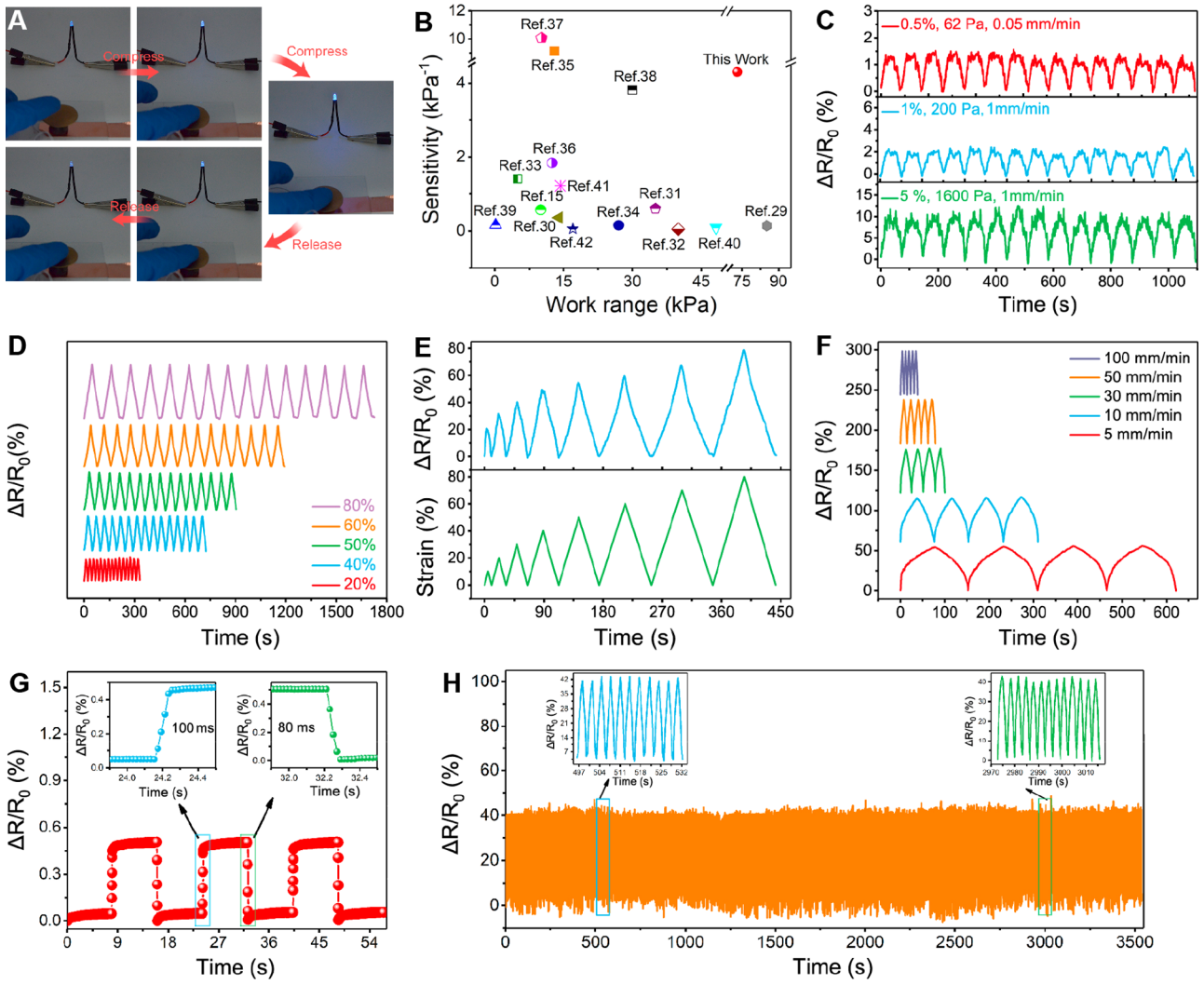

Figure 2. (A) A demonstration showing the conductivity of RPIMX composite aerogel during compressing/releasing. (B) A comparison of the sensitivity and work range between RPIMX pressure sensor and reported sensors. (C,D) Multicycle response curves of the RPIMX sensor under various compressive strains. (E) $\Delta R/R_0$ of the RPIMX sensor under stepwise increased strains from 10% to 80%. (F) $\Delta R/R_0$ of the RPIMX pressure sensor under different compressive rates with a compression strain of 30%. (G) Response/recover times of the RPIMX pressure sensor under 0.5% strain and compression rate of 500 mm min^{-1}. (H) Stability test on the piezoresistive behavior of RPIMX under 30% strain at a compression rate of 10 mm min^{-1} for 1000 cycles (insets are the enlarged compressing/releasing curves).

bidirectional freezing technique to assemble GO nanosheets into a vertically and radially aligned structure, obtained aerogel exhibited superior elasticity and absorption capacity to that of nonoriented counterparts. However, the development of conductive and robust aerogels with ordered radial structures for multiple applications is still a great challenge.

Compared with other polymers, polyimide (PI) with excellent mechanical properties and heat resistance has been widely employed in the construction of high-strength polymeric aerogels.[27,28] In this study, a radially architectured PI/MXene (RPIMX) composite aerogel with vertically and radially aligned porosity, with structural features similar to those of the xylem rays in *Liriodendron* stem, is prepared through the interfacial enhancement of PI and radial ice-templating strategy. On the basis of the temperature gradient and the strong interfacial interaction between MXene flakes and polymer, PI and MXene can be assembled into a continuous and macroscopic aerogel with a radially distributed lamellar structure, which manifests boosted mechanical strength and electrical conductivity in the vertical direction. As a piezoresistive strain sensor, RPIMX aerogel exhibits a wide detection range of 0.1%−80% (60 Pa to 76.5 kPa), short response (100 ms)/recovery (80 ms) times, and excellent long-term cycling stability (30% strain for 1000 cycles). Therefore, prepared RPIMX composite aerogel can be readily used to detect various human motions in real-time. In addition, the biomimetic aligned microstructures of PI/MXene enable itself with excellent water transportation capability and heat absorption properties, which also provides a potential approach for efficient solar steam generation.

DESIGN OF THE XYLEM-INSPIRED AEROGELS

Figure 1A and Figure S14 present the preparation process of RPIMX composite aerogels and the digital photograph of the corresponding radial freezing mold. PAA and MXene flakes can form a strong interfacial interaction during the sol−gel process, which is essential for the formation of a strong and integrated conductive three-dimensional structure. Figure 1B demonstrates that the prepared RPIMX composite aerogel possesses ultralight characteristics and can stay on the top of the

https://doi.org/10.1021/acs.nanolett.2c01486
Nano Lett. 2022, 22, 4560−4568

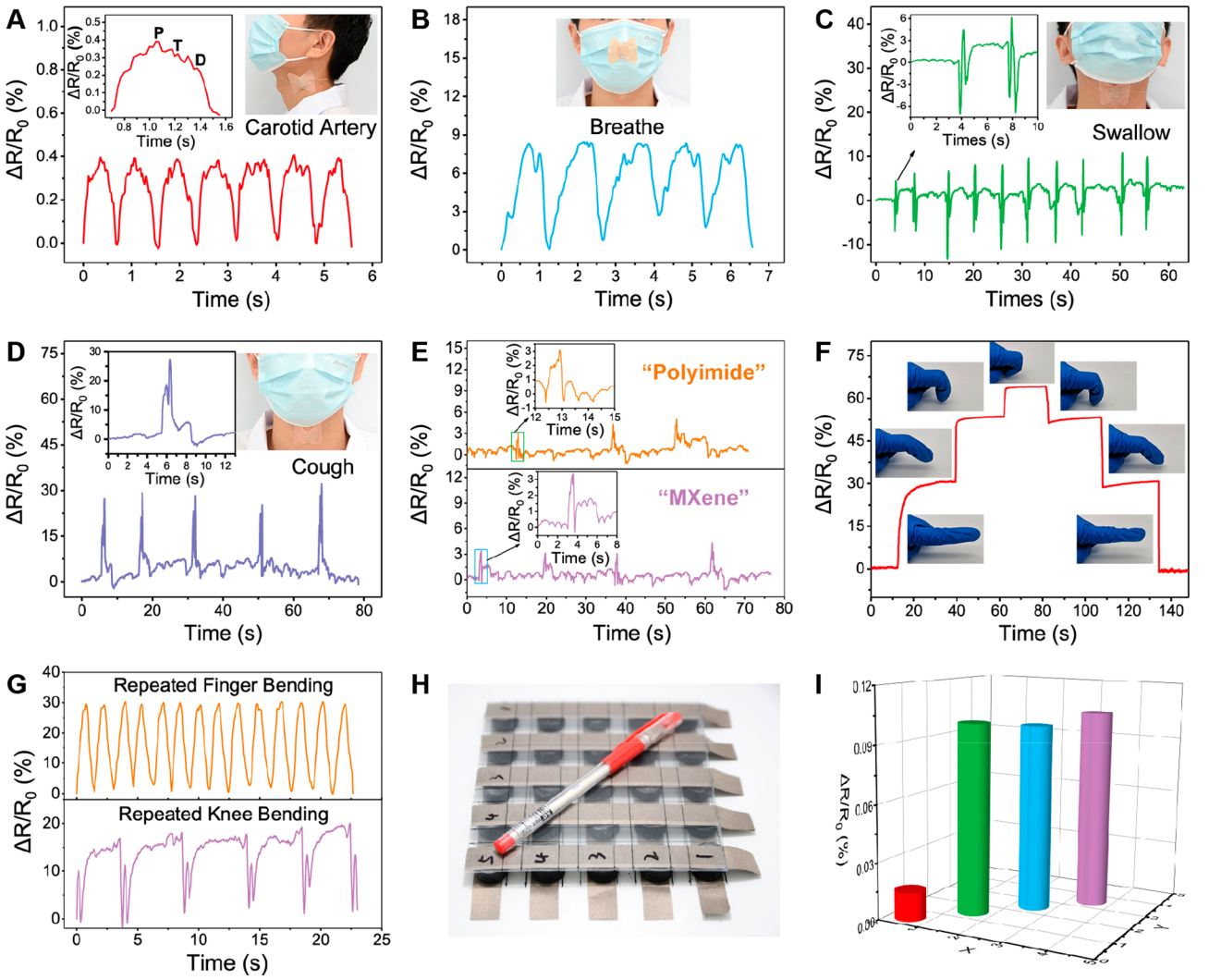

Figure 3. Application of RPIMX aerogel sensor in real-time human motion monitoring: (A−E) Small motion signals of carotid beating, breathing, swallowing, coughing, and words pronunciation. (F-G) Large motion signals of finger bending, knee bending. (H) Photograph of the assembled RPIMX sensor array (5 × 5 pixel), and (I) the corresponding sensing map of the pressure distribution when a ballpoint pen was placed on−the sensor array.

dandelion steadily. The copper tube with a high thermal conductivity as the outer wall can promote the rapid growth of ice crystals from the periphery to the center, and the PVDF board as the base can effectively prevent the ice growth from the bottom to the top, thus resulting in an obvious radial temperature gradient in the device. After the homogeneous PAA/MXene dispersion (Figure S15A) is completely frozen, the ice crystals in the freezing mold can form a significant radial arrangement, trapping the PAA/MXene composites between the radially growing ice crystals (Figure 1C). After the ice crystals are freeze-dried and sublimated by lyophilization, radial porous structures with vertically aligned PAA/MXene lamella akin to the xylem rays of *Liriodendron* stem can be produced (Figure 1D). Subsequently, the RPIMX composite aerogel can be obtained through the final heat-treatment in an argon atmosphere to induce dehydration and cyclization in PAA. The strong interfacial interaction between PI and MXene gives RPIMX composite aerogels excellent flexibility and strength, which can be cut into different thicknesses and shapes according to requirements (Figure S15B).

The optical microscope image of the transverse section of the aerogel (Figure 1E) shows that the RPIMX composite aerogel is arranged radially in a well-defined centrosymmetric pattern. The side view of the cylindrical aerogel shows that the PI/MXene nanosheets are vertically arranged in an ordered layered structure (Figure 1F). Zooming in image of a single PI/MXene layer reveals the typical two-dimensional lamellar structure with a wrinkled surface (Figure 1G), there exist no MXene flakes in the viewport, indicating PI and MXene are perfectly integrated. Combining the evidence in Figure 1E−G, it is speculated that the radially arranged PI/MXene composite lamella is constructed by connected MXene flakes using the polymeric PI as the "glue" (Figure 1H). Additionally, due to the constraint effect of PI/MXene composite lamella, ice crystals shrink in conical shapes as they grow toward to the center. As shown in Figure 1I−L, after the ice crystals sublimate the interlayer spacing (λ) between the PI/MXene lamellae become narrower as they are closer to the center of the assembly. Specifically, the λ of the RPIMX composite aerogel increases from about 17.1 μm (Figure 1J, near the center) to about 30.0 μm (Figure 1K, middle) and finally to

https://doi.org/10.1021/acs.nanolett.2c01486
Nano Lett. 2022, 22, 4560−4568

40.2 μm (Figure 1L, near the edge). Vertically arranged and orderly aligned radial structure resembles the "wall" in the building, thus providing strong support during the compression process and resist compressive stress with gradual bending deformation (Figure 1M, Video S1). Figure 1N vividly depicts the interfacial bonding between the MXene flakes and the PI molecular chains according to detailed structural characterization (discussion can be found in the Supporting Information). The surface of the MXene flakes contain a considerable number of hydroxyl groups, which form hydrogen bonds with the amino and carboxyl groups on the PAA chains, thus facilitating the interfacial enhancing strategy to construct a 3D interconnected network in RPIMX.

PIEZORESISTIVE SENSING PERFORMANCE

Obtained RPIMX aerogel connected in a circuit can effectively adjust the brightness of a LED bulb by pressing and releasing (Figure 2A and Video S2), indicating its great potential in piezoresistive sensors. Considering the outstanding mechanical properties of RPIMX composite aerogel, the comprehensive piezoresistive sensing performance was carefully studied (detailed discussion on mechanical properties and extra discussion on piezoresistive sensing performance can be found in the Supporting Information). The comparison of the pressure sensitivity and working range between RPIMX and other piezoresistive sensors is shown in Figure 2B,[15,29−42] indicating the highly competitive sensing performance of nature-inspired RPIMX aerogel. Figure 2C,D presents the cyclic response behavior of the RPIMX composite aerogel under different compression strains, from which stable and reproducible response patterns are observed for a wide strain range from 0.5% to 80%. Notably, a compression strain as low as 0.5% corresponding to stress lower than 0.01 kPa can be effectively detected by the aerogel pressure sensor, and it is also applicable for detecting large compression strain up to 80%. Meanwhile, the RPIMX sensor shows significant resistance change in the entire strain range of 0.5% ∼ 80%, further verifying its excellent detectability and stability in piezoresistive sensing. The resistance change of RPIMX under gradually increased strains from 10% to 80% is shown in Figure 2E. It can be observed that the maximum $\Delta R/R_0$ at each strain shows an approximately linear relationship with the applied compressive strain, in accordance with the linear resistance-strain response in Figure S10B. Figure 2F displays the resistance change of the aerogel piezoresistive sensor at different tensile speeds under 30% strain. It is implied that the RPIMX sensor delivers stable resistance signals under different compression rates, proving the great stability of the conducting 3D networks in RPIMX composite aerogel. Response and recovery speed are also important indicators for pressure sensors. Because of the quick establishment of the conducting path and great resilience of the radially structured aerogel, the RPIMX pressure sensor exhibits a response time of 100 ms and a recovery time of 80 ms at a transient strain of 0.5% (500 mm min^{-1}) (Figure 2G). Finally, due to the high mechanical strength and compressibility of the composite aerogel, the resistance of RPIMX shows no significant change even after 1000 compression cycles, and the $\Delta R/R_0$ also shows excellent recoverability (Figure 2H). All these results confirm that the RPIMX composite aerogel possesses high repeatability, stability, and long-lasting capability as a piezoresistive sensor.

On the basis of the good resilience, high sensitivity, and large stress detection range of RPIMX composite aerogel, its detection performance toward various human movements is further evaluated. Typically, the composite aerogel was tailored and fabricated into a sensor device, which was attached to human skin to detect various biomechanical activity signals (including vocal cord vibration, carotid artery pulsation, breathing, coughing, swallowing, and so forth). The pressure sensor mounted on the carotid artery of the subject (Figure 3A) shows that the artery beats 75 times per minute (the carotid artery beat rate of a healthy adult is 60−100 beats per minute). The outputted waveform consists of three distinguishable characteristic peaks (inset of Figure 3A): P (percussion wave), T (tidal wave), and D (diastolic wave). The sensor fixed on a surgical mask can effectively detect the pressure change of airflow produced by respiration (Figure 3B). Figure 3C shows that the sensor attached to the lower part of the throat can monitor the contraction and extension motion of the laryngeal knot during swallowing. The muscles at the laryngeal knot will continuously and greatly contract during coughing, thus resulting in the decrease of resistance in the pressure sensor adhered to the subject's throat (Figure 3D). The above trials provide us with simple, low-cost, and efficient methods for real-time and accurate human health monitoring. In addition, based on the compression effect caused by the vibration of the vocal cords, the composite aerogel sensor installed on the throat also can identify the signals of phonation. As shown in Figure 3E, when the tester repeatedly utters the words "Polyimide" and "MXene", reproducible characteristic peaks corresponding to the word syllable will appear in the $\Delta R/R_0$ signal curves. Therefore, piezoresistive sensors based on RPIMX composite aerogel is expected to be a promising candidate in vocal recognition device for speech rehabilitation training.

Benefiting from the large detection range of the radial RPIMX composite aerogel, the sensory device was also attached to different joints of the human body to monitor the large bending motions of fingers and legs. Figure 3F shows that the composite aerogel sensor attached to the knuckle can effectively identify the bending degree of the finger. The intensity of the resistance change increases instantly along with the bending movement, which can return to the initial value with no delay after the finger straightening. In addition, the cyclic bending and recovering of the finger at a fixed angle (45°) also outputted a stable $\Delta R/R_0$ signal (Figure 3G), confirming the great stability of piezoresistive performance. The resistance signal generated by the knee joint is also presented in Figure 3G. Because of the excellent compressibility of the composite aerogel, the resistance change signal can be perfectly repeated even under large-scale deformation during iterative knee bending and stretching. The results demonstrate that the high sensitivity and wide detection range of the RPIMX composite aerogel make it a promising wearable sensor for the real-time detection of human motions. Further, the composite aerogels were used to assemble a 5 × 5 pixel sensor array to detect pressures at different positions (Figure 3H, Figure S16). When a ballpoint pen was placed on the surface of the sensor array, the $\Delta R/R_0$ signal changes correspond to the unevenly distributed weight and the position can be recorded and reflected in the rebuilt sensing map (Figure 3I), indicating the potential of the aerogel sensor in complicated sensory devices.

https://doi.org/10.1021/acs.nanolett.2c01486
Nano Lett. 2022, 22, 4560−4568

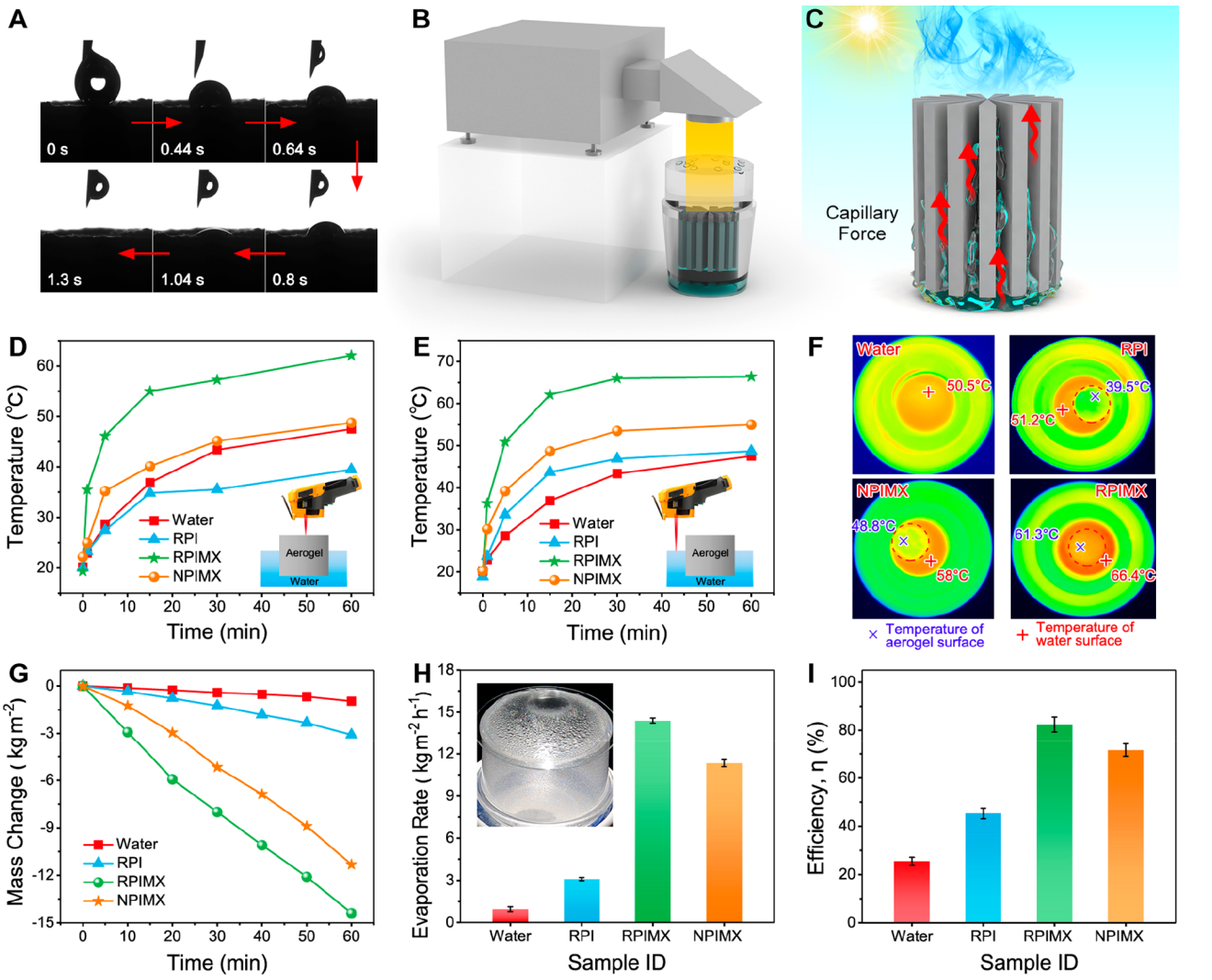

Figure 4. (A) Water contact angle of RPIMX composite aerogel. (B) Schematic illustration of the photothermal evaporation device. (C) Schematic illustration of the capillary force in the aligned channels for efficient water transportation. The temperatures of (D) aerogel surfaces and (E) water surfaces in different evaporation systems. (F) IR images of the RPIMX composite aerogel under 4 sunlight irradiation for 1 h. (G) Time-dependent weight loss of water in different evaporation systems. (H,I) Water evaporation rate and energy efficiency of different evaporation systems.

SOLAR STEAM GENERATION PERFORMANCE

Attributing to the bioinspired aligned channels and local plasmon resonance effect of MXene, RPIMX composite aerogel also possesses excellent water transportation (Figure 4A, Videos S3 and S4, discussion can be found in the Supporting Information) and light-to-heat conversion capabilities.[43] Typically, the water evaporation test was performed using a xenon lamp as the light source, an RPIMX composite aerogel placed in a homemade evaporation system was utilized as the substrate and light absorber (Figure 4B,C). A convex mirror is mounted directly above the aerogel to ensure that the incident light is concentrated on its surface (Figure S17). Figure 4D implies that the surface temperature changes of the aerogel evaporators can be divided into two stages: the first stage (0−30 min) is the heat transfer from aerogel to water after absorbing sunlight, when the speed of heat conversion on the aerogel is much greater than the speed of heat dissipation to the water. In the second stage, the speed of heat conversion is synchronized with the speed of heat dissipation, so the surface temperatures of the aerogels become stable and the constant water evaporation begins.[44] Compared with NPIMX and RPIMX composite aerogels, the pure water and RPI aerogel both exhibit a slower temperature rise during the entire illumination process (Figures 4D−F and S18−S21), the water temperature beside RPI is almost the same as pure water, proving the importance of MXene in photothermal conversion. In addition, RPIMX composite aerogel manifests a significantly enhanced photothermal property than NPIMX, which can be heated to 35.5 °C in 60 s, reaches 55 °C after 15 min, and rises to 61.3 °C after 60 min illumination (Figures 4F and S21). It is noteworthy that the temperatures of the bulk water are higher than those of the evaporators, the difference is especially obvious in RPI and NPIMX (Figure 4E,F). This phenomenon can be explained as follows. Incident light absorbed by the aerogel absorber is converted into heat, which raises the temperature of the water on the upper surface of the aerogel for continuous evaporation. However, part of the heat is inevitably conducted to the bulk water, resulting in the temperature rise of the water reservoir. Additionally, the unremitting water evaporation can rapidly reduce the temperature on the aerogel surface, thus leading to the higher temperature of the bulk water. It is also notable that the

https://doi.org/10.1021/acs.nanolett.2c01486
Nano Lett. 2022, 22, 4560−4568

RPIMX evaporator exhibits a smaller temperature gap (between bulk water and evaporator surface) than other aerogels (Figure 4F), confirming its excellent heat localization capability.

To evaluate the specific evaporation performance of the composite aerogel evaporator system, the weight loss of water under 4 sunlight intensity is recorded in real time (Figure 4G), and the evaporation rate was calculated by deducting the mass change of dark field evaporation. Thanks to the excellent water transport and heat transfer performance, the RPIMX composite aerogel system manifests the largest mass reduction under the same illumination time, showing excellent photothermal evaporation performance. In addition, Figure 4H reveals that the stable evaporation rate of RPIMX aerogel under 4 sunlight intensities is 14.4 kg m^{-2} h^{-1} (20 min), much higher than those of pure water (0.9 kg m^{-2} h^{-1}) and RPI aerogel (3.1 kg m^{-2} h^{-1}). The NPIMX composite aerogel shows a lower evaporation rate (11.3 kg m^{-2} h^{-1}) than that of RPIMX due to its irregular pore distribution. Video S5 and inset of Figure 4H also imply that RPIMX composite aerogel has obvious vapor condensation ability in a short time. The calculated conversion efficiency in Figure 4I further shows that RPIMX has a higher solar energy utilization rate (about 81%) than the other three systems, proving that the combination of MXene and PI, the biomimetic porous structures, and good water transporting properties make RPIMX composite aerogel an excellent photothermal evaporator.

In summary, by mimicking the xylem rays in dicotyledonous stems, lightweight, highly compressible, and radially architectured PI/MXene composite aerogel is prepared by interfacial enhancing strategy and radial ice-templating method, which demonstrate outstanding performance in piezoresistive pressure sensing and photothermal evaporation. Water-soluble polyamic acid (PAA) as the precursor of PI can form a strong interfacial bonding with MXene flakes, thus effectively improving the gelation ability and mechanical strength of the composite aerogel. At the same time, the radial ice-templating strategy can realize the controllable construction of radially aligned lamellar porous structures in the composite aerogel, resulting in excellent mechanical properties and electrical conductivity along the longitudinal direction. As a result, obtained composite aerogel shows a wide detection range of 0.5%−80% strain (60 Pa to 76.5 kPa), excellent pressure sensitivity (4.3 kPa^{-1}), fast piezoresistive responsibility, and great long-term stability when used as a pressure sensor, which can detect various human movements in real-time. The biomimetic radial water transporting channels and light-absorbing MXene components even endow the aerogel with excellent photothermal evaporation performance with a water evaporation rate of 14.4 kg m^{-2} h^{-1} under the irradiation of 4 sunlight intensities. Hence, the great mechanical strength, excellent piezoresistive sensing capability, and light-to-heat conversion performance make RPIMX composite aerogels promising candidates for flexible/wearable piezoresistive sensors and solar evaporators.

■ ASSOCIATED CONTENT

Supporting Information

The Supporting Information is available free of charge at https://pubs.acs.org/doi/10.1021/acs.nanolett.2c01486.

Additional experimental materials and methods, supplementary discussion on XRD, Raman, FTIR, XPS, and TGA characterizations, discussion on the morphology of other aerogels, detailed discussion on mechanical properties, extra discussion on piezoresistive sensing performance, water transport, and thermal insulation capabilities (PDF)

Video S1: Compression test (MP4)

Video S2: Conductivity test (MP4)

Video S3: Dynamic water contact angle (MP4)

Video S4: Water absorbing tests (MP4)

Video S5: Photothermal evaporation test (MP4)

■ AUTHOR INFORMATION

Corresponding Authors

Yunpeng Huang − *Key Laboratory of Synthetic and Biological Colloids, Ministry of Education, School of Chemical and Material Engineering, Jiangnan University, Wuxi 214122, China;* orcid.org/0000-0002-8710-9062; Email: hypjnu@jiangnan.edu.cn

Tianxi Liu − *Key Laboratory of Synthetic and Biological Colloids, Ministry of Education, School of Chemical and Material Engineering, Jiangnan University, Wuxi 214122, China*; Email: txliu@jiangnan.edu.cn

Authors

Lei Pu − *Key Laboratory of Synthetic and Biological Colloids, Ministry of Education, School of Chemical and Material Engineering, Jiangnan University, Wuxi 214122, China*

Haojie Ma − *Key Laboratory of Synthetic and Biological Colloids, Ministry of Education, School of Chemical and Material Engineering, Jiangnan University, Wuxi 214122, China*

Jiancheng Dong − *Key Laboratory of Synthetic and Biological Colloids, Ministry of Education, School of Chemical and Material Engineering, Jiangnan University, Wuxi 214122, China*

Chao Zhang − *State Key Laboratory for Modification of Chemical Fibers and Polymer Materials, College of Materials Science and Engineering, Donghua University, Shanghai 201620, China;* orcid.org/0000-0003-1255-7183

Feili Lai − *Department of Chemistry, KU Leuven, Leuven 3001, Belgium;* orcid.org/0000-0002-4945-0737

Guanjie He − *Christopher Ingold Laboratory, Department of Chemistry, University College London, London WC1H 0AJ, United Kingdom;* orcid.org/0000-0002-7365-9645

Piming Ma − *Key Laboratory of Synthetic and Biological Colloids, Ministry of Education, School of Chemical and Material Engineering, Jiangnan University, Wuxi 214122, China;* orcid.org/0000-0002-4597-0639

Weifu Dong − *Key Laboratory of Synthetic and Biological Colloids, Ministry of Education, School of Chemical and Material Engineering, Jiangnan University, Wuxi 214122, China;* orcid.org/0000-0002-7432-8362

Complete contact information is available at: https://pubs.acs.org/10.1021/acs.nanolett.2c01486

Author Contributions

The manuscript was written through contributions of all authors. All authors have given approval to the final version of the manuscript.

Notes

The authors declare no competing financial interest.

https://doi.org/10.1021/acs.nanolett.2c01486
Nano Lett. 2022, 22, 4560−4568

■ ACKNOWLEDGMENTS

This work is financially supported by the National Natural Science Foundation of China (No. 21875033), the Shanghai Scientific and Technological Innovation Project (No.18JC1410600), the Program of the Shanghai Academic Research Leader (No.17XD1400100), and the State Key Laboratory for Modification of Chemical Fibers and Polymer Materials (Donghua University).

■ REFERENCES

(1) Dong, J.; Wang, D.; Peng, Y.; Zhang, C.; Lai, F.; He, G.; Ma, P.; Dong, W.; Huang, Y.; Parkin, I. P.; Liu, T. Ultra-stretchable and superhydrophobic textile-based bioelectrodes for robust self-cleaning and personal health monitoring. *Nano Energy* **2022**, *97*, 107160.

(2) Wang, X.; Tao, L.; Yuan, M.; Wang, Z.; Yu, J.; Xie, D.; Luo, F.; Chen, X.; Wong, C. Sea urchin-like microstructure pressure sensors with an ultra-broad range and high sensitivity. *Nat. Commun.* **2021**, *12*, 1776.

(3) Wan, K.; Liu, Z.; Schroeder, B. C.; Chen, G.; Santagiuliana, G.; Papageorgiou, D. G.; Zhang, H.; Bilotti, E. Highly stretchable and sensitive self-powered sensors based on the N-type thermoelectric effect of polyurethane/nax(Ni-ett)n/graphene oxide composites. *Compos. Commun.* **2021**, *28*, 100952.

(4) Jang, J.; Kim, H.; Ji, S.; Kim, H. J.; Kang, M. S.; Kim, T. S.; Won, J. E.; Lee, J. H.; Cheon, J.; Kang, K.; Im, W. B.; Park, J. U. Mechanoluminescent, air-dielectric MoS_2 transistors as active-matrix pressure sensors for wide detection ranges from footsteps to cellular motions. *Nano Lett.* **2020**, *20*, 66−74.

(5) Lamport, Z. A.; Cavallari, M.; Kam, K. A.; McGinn, C. K.; Yu, C.; Kymissis, I. Organic thin film transistors in mechanical sensors. *Adv. Funct. Mater.* **2020**, *30*, 2004700.

(6) Wu, Y.; Chen, E.; Weng, X.; He, Z.; Chang, G.; Pan, X.; Liu, J.; Huang, K.; Huang, K.; Lei, M. Conductive polyvinyl alcohol/silver nanoparticles hydrogel sensor with large draw ratio, high sensitivity and high stability for human behavior monitoring. *Eng. Sci.* **2022**, *18*, 113−120.

(7) Wang, X.; Lu, J.; Lu, S.; Li, B.; Zhang, L.; Ma, C.; Ma, K.; Lin, L.; Jiang, X.; Yang, B. Health monitoring of repaired composite structure using MXene sensor. *Compos. Commun.* **2021**, *27*, 100850.

(8) Ti, C.; Ari, A. B.; Karakan, M. C.; Yanik, C.; Kaya, I. I.; Hanay, M. S.; Svitelskiy, O.; Gonzalez, M.; Seren, H.; Ekinci, K. L. Frequency-dependent piezoresistive effect in top-down fabricated gold nanoresistors. *Nano Lett.* **2021**, *21*, 6533−6539.

(9) Fan, M.; Wu, L.; Hu, Y.; Qu, M.; Yang, S.; Tang, P.; Pan, L.; Wang, H.; Bin, Y. A highly stretchable natural rubber/buckypaper/natural rubber (NR/N-BP/NR) sandwich strain sensor with ultrahigh sensitivity. *Adv. Compos. Hybrid Mater.* **2021**, *4*, 1039−1047.

(10) Meng, K.; Xiao, X.; Wei, W.; Chen, G.; Nashalian, A.; Shen, S.; Chen, J. Wearable pressure sensors for pulse wave monitoring. *Adv. Mater.* **2022**, No. e2109357.

(11) Li, R.; Tian, X.; Wei, M.; Dong, A.; Pan, X.; He, Y.; Song, X.; Li, H. Flexible pressure sensor based on cigarette filter and highly conductive MXene sheets. *Compos. Commun.* **2021**, *27*, 100889.

(12) Dong, J.; Li, L.; Zhang, C.; Ma, P.; Dong, W.; Huang, Y.; Liu, T. Ultra-highly stretchable and anisotropic SEBS/F127 fiber films equipped with an adaptive deformable carbon nanotube layer for dual-mode strain sensing. *J. Mater. Chem. A* **2021**, *9*, 18294−18305.

(13) Shen, Z.; Zhu, X.; Majidi, C.; Gu, G. Cutaneous ionogel mechanoreceptors for soft machines, physiological sensing, and amputee prostheses. *Adv. Mater.* **2021**, *33*, No. 2102069.

(14) Chakraborty, P.; Guterman, T.; Adadi, N.; Yadid, M.; Brosh, T.; Adler-Abramovich, L.; Dvir, T.; Gazit, E. A self-healing, all-organic, conducting, composite peptide hydrogel as pressure sensor and electrogenic cell soft substrate. *ACS Nano* **2019**, *13*, 163−175.

(15) Khan, F. A.; Ajmal, C. M.; Bae, S.; Seo, S.; Moon, H.; Baik, S. Silver nanoflower decorated graphene oxide sponges for highly sensitive variable stiffness stress sensors. *Small* **2018**, *14*, No. 1800549.

(16) Wang, G.; Liao, X.; Zou, F.; Song, P.; Tang, W.; Yang, J.; Li, G. Flexible TPU/MWCNTs/BN composites for frequency-selective electromagnetic shielding and enhanced thermal conductivity. *Compos. Commun.* **2021**, *28*, 100953.

(17) Ren, H.; Zheng, L.; Wang, G.; Gao, X.; Tan, Z.; Shan, J.; Cui, L.; Li, K.; Jian, M.; Zhu, L.; Zhang, Y.; Peng, H.; Wei, D.; Liu, Z. Transfer-medium-free nanofiber-reinforced graphene film and applications in wearable transparent pressure sensors. *ACS Nano* **2019**, *13*, 5541−5548.

(18) Liu, H.; Dong, M.; Huang, W.; Gao, J.; Dai, K.; Guo, J.; Zheng, G.; Liu, C.; Shen, C.; Guo, Z. Lightweight conductive graphene/thermoplastic polyurethane foams with ultrahigh compressibility for piezoresistive sensing. *J. Mater. Chem. C* **2017**, *5*, 73−83.

(19) Wu, Y.-H.; Liu, H.-Z.; Chen, S.; Dong, X.-C.; Wang, P.-P.; Liu, S.-Q.; Lin, Y.; Wei, Y.; Liu, L. Channel crack-designed gold@PU sponge for highly elastic piezoresistive sensor with excellent detectability. *ACS Appl. Mater. Interfaces* **2017**, *9*, 20098−20105.

(20) Chang, K.; Li, L.; Zhang, C.; Ma, P.; Dong, W.; Huang, Y.; Liu, T. Compressible and robust PANI sponge anchored with erected MXene flakes for human motion detection. *Compos. Part A Appl. Sci. Manuf.* **2021**, *151*, 106671.

(21) Wei, X.; Cao, X.; Wang, Y.; Zheng, G.; Dai, K.; Liu, C.; Shen, C. Conductive herringbone structure carbon nanotube/thermoplastic polyurethane porous foam tuned by epoxy for high performance flexible piezoresistive sensor. *Compos. Sci. Technol.* **2017**, *149*, 166−177.

(22) Liu, Y.; Wang, D.; Zhang, C.; Zhao, Y.; Ma, P.; Dong, W.; Huang, Y.; Liu, T. Compressible and lightweight MXene/carbon nanofiber aerogel with "layer-strut" bracing microscopic architecture for efficient energy storage. *Adv. Fiber Mater.* **2022**.

(23) Liu, D.; Dong, X.; Han, B.; Huang, H.; Qi, M. Cellulose nanocrystal/collagen hydrogels reinforced by anisotropic structure: shear viscoelasticity and related strengthening mechanism. *Compos. Commun.* **2020**, *21*, 100374.

(24) Li, Q.; Yuan, Z.; Zhang, C.; Hu, S.; Chen, Z.; Wu, Y.; Chen, P.; Qi, H.; Ye, D. Tough, highly oriented, super thermal insulating regenerated all-cellulose sponge-aerogel fibers integrating a graded aligned nanostructure. *Nano Lett.* **2022**, DOI: 10.1021/acs.nanolett.1c03943.

(25) Chen, L.; Ding, L.; Liu, K.; Mao, Z.; Wang, B.; Feng, X.; Sui, X. Lightweight, environmentally friendly, and underwater superelastic 3D-architectured aerogels for efficient protein separation. *ACS Sustainable Chem. Eng.* **2021**, *9*, 11738−11747.

(26) Wang, C.; Chen, X.; Wang, B.; Huang, M.; Wang, B.; Jiang, Y.; Ruoff, R. S. Freeze-casting produces a graphene oxide aerogel with a radial and centrosymmetric structure. *ACS Nano* **2018**, *12*, 5816−5825.

(27) Gouzman, I.; Grossman, E.; Verker, R.; Atar, N.; Bolker, A.; Eliaz, N. Advances in polyimide-based materials for space applications. *Adv. Mater.* **2019**, *31*, No. 1807738.

(28) Zhang, Q.; Han, Y.; Ding, X.; Zhang, P.; Wang, Y.; Shu, M.; Gong, Y.; Zheng, K.; Tian, X.; Zhang, X. A simple strategy to prepare functional PI microspheres by constructing coating on PAA microspheres followed thermal imidization reaction. *Compos. Commun.* **2021**, *24*, 100642.

(29) Liu, H.; Chen, X.; Zheng, Y.; Zhang, D.; Zhao, Y.; Wang, C.; Pan, C.; Liu, C.; Shen, C. Lightweight, superelastic, and hydrophobic polyimide nanofiber/MXene composite aerogel for wearable piezoresistive sensor and oil/water separation applications. *Adv. Funct. Mater.* **2021**, *31*, 2008006.

(30) Yang, J.; Ye, Y.; Li, X.; Lü, X.; Chen, R. Flexible, conductive, and highly pressure-sensitive graphene-polyimide foam for pressure sensor application. *Compos. Sci. Technol.* **2018**, *164*, 187−194.

(31) He, X.; Liu, Q.; Zhong, W.; Chen, J.; Sun, D.; Jiang, H.; Liu, K.; Wang, W.; Wang, Y.; Lu, Z.; Li, M.; Liu, X.; Wang, X.; Sun, G.; Wang, D. Strategy of constructing light-weight and highly compressible graphene-based aerogels with an ordered unique configuration for wearable piezoresistive sensors. *ACS Appl. Mater. Interfaces* **2019**, *11*, 19350−19362.

https://doi.org/10.1021/acs.nanolett.2c01486
Nano Lett. 2022, 22, 4560−4568

(32) Zhu, L.; Wang, Y.; Mei, D.; Wu, X. Highly sensitive and flexible tactile sensor based on porous graphene sponges for distributed tactile sensing in monitoring human motions. *J. Microelectromech. Syst.* **2019**, *28*, 154−163.
(33) Huang, J.; Li, D.; Zhao, M.; Ke, H.; Mensah, A.; Lv, P.; Tian, X.; Wei, Q. Flexible electrically conductive biomass-based aerogels for piezoresistive pressure/strain sensors. *Chem. Eng. J.* **2019**, *373*, 1357−1366.
(34) Ge, G.; Cai, Y.; Dong, Q.; Zhang, Y.; Shao, J.; Huang, W.; Dong, X. A flexible pressure sensor based on rGO/polyaniline wrapped sponge with tunable sensitivity for human motion detection. *Nanoscale* **2018**, *10*, 10033−10040.
(35) Huang, J.; Zeng, J.; Liang, B.; Wu, J.; Li, T.; Li, Q.; Feng, F.; Feng, Q.; Rood, M. J.; Yan, Z. Multi-arch-structured all-carbon aerogels with superelasticity and high fatigue resistance as wearable sensors. *ACS Appl. Mater. Interfaces* **2020**, *12*, 16822−16830.
(36) Wang, M.; Chen, Y.; Qin, Y.; Wang, T.; Yang, J.; Xu, F. Compressible, fatigue resistant, and pressure-sensitive carbon aerogels developed with a facile method for sensors and electrodes. *ACS Sustainable Chem. Eng.* **2019**, *7*, 12726−12733.
(37) Long, S.; Feng, Y.; He, F.; Zhao, J.; Bai, T.; Lin, H.; Cai, W.; Mao, C.; Chen, Y.; Gan, L.; Liu, J.; Ye, M.; Zeng, X.; Long, M. Biomass-derived, multifunctional and wave-layered carbon aerogels toward wearable pressure sensors, supercapacitors and triboelectric nanogenerators. *Nano Energy* **2021**, *85*, 105973.
(38) Guo, Y.; Zhong, M.; Fang, Z.; Wan, P.; Yu, G. A wearable transient pressure sensor made with MXene nanosheets for sensitive broad-range human-machine interfacing. *Nano Lett.* **2019**, *19*, 1143−1150.
(39) Xu, X.; Wang, R.; Nie, P.; Cheng, Y.; Lu, X.; Shi, L.; Sun, J. Copper nanowire-based aerogel with tunable pore structure and its application as flexible pressure sensor. *ACS Appl. Mater. Interfaces* **2017**, *9*, 14273−14280.
(40) Tewari, A.; Gandla, S.; Bohm, S.; McNeill, C. R.; Gupta, D. Highly exfoliated MWNT-rGO ink-wrapped polyurethane foam for piezoresistive pressure sensor applications. *ACS Appl. Mater. Interfaces* **2018**, *10*, 5185−5195.
(41) Wu, X.; Liu, X.; Wang, J.; Huang, J.; Yang, S. Reducing structural defects and oxygen-containing functional groups in GO-hybridized CNTs aerogels: Simultaneously improve the electrical and mechanical properties to enhance pressure sensitivity. *ACS Appl. Mater. Interfaces* **2018**, *10*, 39009−39017.
(42) Zhao, X.; Wang, W.; Wang, Z.; Wang, J.; Huang, T.; Dong, J.; Zhang, Q. Flexible PEDOT:PSS/polyimide aerogels with linearly responsive and stable properties for piezoresistive sensor applications. *Chem. Eng. J.* **2020**, *395*, 125115.
(43) Zhao, X.; Peng, L.-M.; Tang, C.-Y.; Pu, J.-H.; Zha, X.-J.; Ke, K.; Bao, R.-Y.; Yang, M.-B.; Yang, W. All-weather-available, continuous steam generation based on the synergistic photo-thermal and electro-thermal conversion by MXene-based aerogels. *Mater. Horiz.* **2020**, *7*, 855−865.
(44) Zhao, L.; Bhatia, B.; Yang, S.; Strobach, E.; Weinstein, L. A.; Cooper, T. A.; Chen, G.; Wang, E. N. Harnessing heat beyond 200 °C from unconcentrated sunlight with nonevacuated transparent aerogels. *ACS Nano* **2019**, *13*, 7508−7516.

https://doi.org/10.1021/acs.nanolett.2c01486
Nano Lett. 2022, 22, 4560−4568